AIAA 2001-2702
Spatial Linear Instability of Confluent Wake/Boundary Layers

William W. Liou and Fengjun Liu
Dept. of Mechanical and Aeronautical Engineering
Western Michigan University
Kalamazoo, MI

31st AIAA Fluid Dynamics Conference & Exhibit
11-14 June 2001/Anaheim, CA

AIAA-2001-2702

Spatial Linear Instability of Confluent Wake/Boundary Layers

William W. Liou* and Fengjun Liu**

Department of Mechanical and Aeronautical Engineering
Western Michigan University
Kalamazoo, MI 49008

Abstract

The spatial linear instability of incompressible confluent wake/boundary layers is analyzed. The flow model adopted is a superposition of the Blasius boundary layer and a wake located above the boundary layer. The Orr-Sommerfeld equation is solved using a global numerical method for the resulting eigenvalue problem. The numerical procedure is validated by comparing the present solutions for the instability of the Blasius boundary layer and for the instability of a wake with published results. For the confluent wake/boundary layers, modes associated with the boundary layer and the wake, respectively, are identified. The boundary layer mode is found amplified as the wake approaches the wall. On the other hand, the modes associated with the wake, including a symmetric mode and an antisymmetric mode, are stabilized by the reduced distance between the wall and the wake. An unstable mode switching at low frequency is observed where the antisymmetric mode becomes more unstable than the symmetric mode when the wake velocity defect is high.

1. Introduction

The linear instability of the boundary layer developed along a flat plate is a classical problem[1] in hydrodynamic stability and has been studied by many authors. The disturbances obtained by the solution of the Orr-Sommerfeld equation have been found useful and reliable in describing many different fluid flow phenomena such as the initial stage of natural flow transition in the boundary layer[2] and the bursting of the streamwise coherent structures in turbulent boundary layers[3].

Possibly just as widely studied as the boundary layer instability, the instability of wake flows is another classical analysis examined by many reports[4-7]. Two amplifying modes are often identified, a symmetric and an antisymmetric modes. For a near wake[5], the symmetric mode was found to have a higher spatial growth rate and was observed in the experiment. An instability analysis of the wakes embedded in a boundary layer was studied in Bajwa[8] for the modeling of the presence of particles in bounded and unbounded shear flows. Absolute instability was found to occur for sufficiently large values of the centerline wake defect[6].

This study is concerned with the linear instability of confluent wake/boundary layer flows. The confluent wake/boundary layer is among the flow phenomena observed in the complex flow field around multi-element airfoils. For instance, for a three-element airfoil the slat and the flap element may be deployed and extended away from the main element in a landing or a take-off configurations. The wake generated by a proceeding element, such as the slat, appears above the succeeding element, or the main element. The interaction of the confluent wake and boundary layer occurs over a significant portion of the main element. Experiments[9-13] have shown that the confluent wake /boundary layer can exhibit entirely different behavior, depending upon the operating conditions, such as the Reynolds number and the relative positions between the elements. This change causes dramatic variation in boundary layer transition[10,11] and its aerodynamic performance[12,13]. There are also evidence suggesting that the physics of the flow in the slat near wake region above the main element is critical to the flow noise generated by multi-element airfoils[14].

Due in part to the high Reynolds numbers, it is difficult and expensive to experimentally examine the flow in detail. Computational studies based on the Reynolds-averaged Navier-Stokes equations of such flows[15,16] suggest that the mean or average quantities can be obtained that agree satisfactorily with measured data.

*Associate Professor, Senior Member AIAA.
**Graduate Assistant

In this study, the characteristics of small disturbances in the confluent near wake and boundary layer are investigated. The flow model considered consists of a wake located above the Blasius boundary layer. The base flow velocity profile adopted represents a reasonable approximation to the measured[9] and the calculated[15] mean velocity profiles in the confluent near wake/boundary layer region over a multi-element airfoil. The amplitudes of the disturbances are assumed small such that a linearized form of the Navier-Stokes equations can be used. A global numerical solution technique[17,18,19] is applied in this study. The global method is capable of predicting the entire eigenvalue spectrum, including the discrete and the continuous parts, which is important to the current studies. As will be shown in the results, multiple discrete modes associated with the boundary layer and wake flow can appear and a global approximation is more desirable a method to use than the traditional local shooting method. As a result, the study establishes a link, based on a linear analysis, between the modes for confluent wake and laminar boundary layer, which often proceeds that with transitional and turbulent boundary layer in the flow over multi-element airfoils.

The Orr-Sommerfeld equation will be briefly derived in the following section. It is followed by a description of the base velocity profile and the global method of solution.

2. Formulation and Method of Solution

Stability Equation

The flow geometry considered is shown in Figure 1. The two-dimensional incompressible confluent wake/boundary layer is described in the Cartesian coordinate system, (x^*, y^*, z^*). The instantaneous value of a flow variable, ϕ^*, is decomposed into a time-independent component denoted by the upper case and a fluctuation denoted by a prime. That is ,

$$\begin{aligned} u^*(x^*,y^*,z^*,t^*) &= u'^*(x^*,y^*,z^*,t^*) + U^*(y^*) \\ v^*(x^*,y^*,z^*,t^*) &= v'^*(x^*,y^*,z^*,t^*) \\ w^*(x^*,y^*,z^*,t^*) &= w'^*(x^*,y^*,z^*,t^*) \\ p^*(x^*,y^*,z^*,t^*) &= p'^*(x^*,y^*,z^*,t^*) \end{aligned} \quad (1)$$

where u^*, v^*, and w^* are the velocity components in the x^*, y^*, and z^* directions, respectively. p^* denotes pressure.

For simplicity, the parallel flow assumption, commonly used in hydrodynamic stability analyses, is applied. This approximation results in the leading-order problem in a multiple scale method that includes the effects of the slow flow divergence[20]. Thus, in the current analysis, the nonparallel effects are not considered. The continuity and the momentum equations are nondimensionalized by using the displacement thickness of the boundary layer, δ^*, as the length scale and the velocity of the free stream, u_∞^*, as the velocity scale and linearized about the base flow. Separable solutions are then sought for the fluctuations in the non-dimensional form,

$$\begin{Bmatrix} u' \\ v' \\ w' \\ p' \end{Bmatrix} = \begin{Bmatrix} u(y) \\ v(y) \\ w(y) \\ p(y) \end{Bmatrix} \exp[i(\alpha x - \omega t)] \quad (2)$$

The u, w, and p variables may be eliminated from the linearized equations and the Orr-Sommerfeld equation for the cross-stream velocity perturbation, $v(y)$, can be given by,

$$[i(\alpha U - \omega)(\frac{d^2}{dy^2} - \alpha^2) - i\alpha\frac{d^2U}{dy^2} - \frac{1}{R_e^*}(\frac{d^2}{dy^2} - \alpha^2)^2]v = 0 \quad (3)$$

Equation (3) governs the mode shape of wavelike disturbances associated with the base profile in terms of the streamwise wavenumber, α, the wave frequency, ω, and the flow Reynolds number, $R_e^*(=\frac{u_\infty^*\delta^*}{\nu})$. The boundary conditions for v are,

$$v = \frac{dv}{dy} = 0 \quad \text{at } y = 0,\ \infty \quad (4)$$

Base Flow Velocity Profiles

The flow model depicted in Figure 1 consists of two separate regions where flow shearing can occur. They are the region near the wall where the boundary layer develops and the region away from the wall where the wake generated by an upstream element is located. The Blasius velocity profile is used for the boundary layer. The wake profile is defined by

$$U = 1.0 - a\exp(-0.5(y-h)^2) \quad (5)$$

where a represents the wake velocity defect and h the wake height, or the distance between the wake and the wall. Equation (5) closely mimics measured wake velocity profile[5] and is a reasonable analytical expression to use in the current study. The base flow velocity is obtained by a superposition of the Blasius velocity profile and equation (5). A similar superposition of the velocity profiles has also been used in the convective stability analysis[8] of a wake embedded in the Blasius boundary layer. Care has been taken to ensure that

no discontinuities exist in the second derivative of the resulting velocity distribution, $\frac{d^2U}{dy^2}$.

Equations (3), (4), and (5) define an eigenvalue problem. In the spatial instability analysis described here, the complex wave number, α, is the eigenvalue and the frequency, ω, is taken to be real. Solutions are sought as the disturbances develop spatially downstream.

Numerical Scheme

The Orr-Sommerfeld equation (3) is integrated numerically using a global method based on sixth - order accuracy finite difference formulae. The grid node distribution in the physical domain allows for high node density in the high shear regions near the wall and in the wake according to

$$y_i^* = y_1^* + \theta(y_n^* - y_1^*) \tag{6}$$

where

$$\theta = \frac{\eta}{\xi} + \frac{1}{\gamma\xi}\tanh\left[(\xi\frac{i-1}{n-1} - \eta)(0.5\ln\frac{1+\gamma}{1-\gamma})\right]$$

$\xi = 1,\ \eta = 1,$ for clustering near y_1^*

$\xi = 1,\ \eta = 0,$ for clustering near y_n^*

$\xi = 2,\ \eta = 1,$ for clustering near y_1^* and y_n^*

γ is a clustering coefficient that ranges between 0 and 1. The discretization of equation (3) using the finite difference method results in a system of homogeneous equations nonlinear in the parameter, α,

$$D_4(\alpha)v = 0 \tag{7}$$

The matrix, D_4, is a lambda matrix of degree four[21] and can be expressed as a scalar polynomial with matrix coefficients,

$$D_4(\alpha) = C_0\alpha^4 + C_1\alpha^3 + C_2\alpha^2 + C_3\alpha + C_4 \tag{8}$$

With the inclusion of the boundary conditions, the matrices C's are square matrices of order n which represents the number of grid point in y. A linear companion matrix method has been used to linearize the lambda matrix. The resulting general eigenvalue problem becomes

$$\{E - \alpha F\}V = 0 \tag{9}$$

where

$$E = \begin{pmatrix} -C_1 & -C_2 & -C_3 & -C_4 \\ I & 0 & 0 & 0 \\ 0 & I & 0 & 0 \\ 0 & 0 & I & 0 \end{pmatrix}$$

$$F = \begin{pmatrix} C_0 & 0 & 0 & 0 \\ 0 & I & 0 & 0 \\ 0 & 0 & I & 0 \\ 0 & 0 & 0 & I \end{pmatrix}$$

and

$$V = \begin{pmatrix} \alpha^3 v \\ \alpha^2 v \\ \alpha\ v \\ v \end{pmatrix}$$

Equation (9) can be further transformed to an algebraic eigenvalue problem seeking the eigenvalues of matrix A,

$$A = \begin{pmatrix} -C_0^{-1}C_1 & -C_0^{-1}C_2 & C_0^{-1}C_3 & C_0^{-1}C_4 \\ I & 0 & 0 & 0 \\ 0 & I & 0 & 0 \\ 0 & 0 & I & 0 \end{pmatrix} \tag{10}$$

The eigenvalues may be obtained by using QR or QZ algorithms. The details of the formulation and the application of the Linear Companion Matrix method can be found in references 17,19, and 21.

The solver is validated by comparing the eigenvalue with reported data for the Blasius boundary layer and wakes, respectively. The results of the code validation and spatial instability calculations for the model confluent wake/boundary layer are presented in the next section.

3. Results and Discussions

Table 1 shows a comparison of the calculated eigenvalue with that of Jordinson[22] for the Blasius boundary layer. The present values agree well with the data, particularly for cases with a high number of grid points, N. To validate the current numerical solver for the wake flow, a measured wake profile[5] is placed at h = 20 and the boundary layer removed from the viscous wall. Figure 2 shows a comparison of the dispersion relationship obtained by using the present numerical solver and that reported[5] for both the symmetric and the antisymmetric modes, based on the cross-stream velocity purturbance, v. The results obtained by using the current global method with N = 300 agree well with the previous calculation, which is based on a local shooting

method. The results show that the global numerical solver used in the current study is accurately capturing the wake and the boundary layer instabilities. In the following, the instability modes associated with the model confluent wake/boundary layer flow are examined.

The flow model used in the present analysis is shown in Figure 1. Figure 3 shows the spectrum of the wave speed for the model confluent wake/boundary layer flow with $R_e^* = 998$ and $\omega = 0.1122$. The wake height, h, is 20, the width is 4.83, and the wake maximum velocity defect, a, is 0.6. For comparison, the wave speed spectrum for the Blasius boundary layer alone with the same R_e^* and ω is also included. In addition to the boundary layer mode, two discrete unstable modes appear in the case of the confluent wake/boundary layer, which are identified as Wake Mode 1 and Wake Mode 2. Modes 1 and 2 correspond to the symmetric and the antisymmetric modes found in the linear stability of the wake flows, respectively. The presence of the wake above the boundary layer at this height apparently has no significant effects on the continuous part of the eigenvalue spectrum. In the following, the discrete unstable modes in the confluent wake/boundary layer will be examined in details as they are linearly unstable and are likely to be physically observed.

Figure 4 shows the neutral curve of the boundary layer mode with $h = 7.14$ and $a = 0.6$. The neutral curve for the Blasius boundary layer[22] is also included for comparison. The presence of the wake has resulted in a significant decrease of the critical Reynolds number. The value is 445 for the present case, compared to 520 for the Blasius boundary layer. The neutral curve moves up slightly for all Reynolds numbers with more significant changes in the high frequency range near the critical point. As can be seen from Figure 5, which shows the variation of the spatial growth rate, $-\alpha_i$, with frequency for $R_e^* = 998$, the neutral frequencies increase as the wake is brought closer to the wall. Figure 5 also shows that the maximum growth rate of the unstable boundary layer mode increases with the reduced distance between the wake and the wall.

To examine the effect of h on the boundary layer mode shape, the eigenfunctions for a frequency of $\omega = 0.1122$, which roughly corresponds to the most unstable frequency, are calculated and their real parts are presented in Figure 6. The eigenfunctions have been normalized by their respective maximum amplitudes. The eigenfunction of the boundary layer mode decays faster away from the wall as the wakes become situated closer to the wall. The damping effect of the wake on the eigenfunction of the boundary layer mode is quite significant in the region above the wake.

The velocity defect of the wake in the model problem is determined by the value of a, which also determines the shear strength for a constant wake width. Figure 7 shows the change in the growth rate of the $\omega = 0.1122$ boundary layer mode with the wake velocity defect and wake height. The growth rate for such a mode in the Blasius boundary layer, –0.0057, is indicated in the figure. Figure 7 shows that the amplifying effect of the reduced wake height on the growth rate of the boundary layer mode, as is discussed above, becomes more pronounced as the velocity defect of the wake increases. For example, when the value of h is about 6, there is an increase of 400% for the growth rate for $a = 0.8$, as compared to about 40% for $a = 0.2$. It should be noted that the lowest value of the centerline velocity defect for a Gausian wake profile to exhibit absolute instability is 0.946[6].

In addition to the boundary layer mode, the eigenvalue spectrum for the confluent wake/boundary layer, shown in Figure 3, also contains two discrete, unstable modes that are directly associated with the wake. These modes have been identified as Wake Modes 1 and 2. As is discussed above, the Mode 1 disturbances are symmetric with respect to the wake center, where the velocity defect is the maximum, and Mode 2 represents antisymmetric disturbances. Figure 8 shows the variations of the spatial growth rates of Mode 1 and Mode 2 with wake height h and velocity defect a. The Reynolds number is 998 and $\omega = 0.1122$. The growth rates for Mode 1 and Mode 2 are both seen to decrease as h decreases. This appears true for the different value of the velocity defect selected, from 0.2 to 0.8, with more prominent decreases for the high-defect cases. Note that the boundary layer mode, as shown in Figure 7, becomes more unstable as the wake is placed closer to the wall. Therefore, the reduced distance between the wall and the wake has an amplifying effect on the boundary layer mode, but a damping effect on the wake modes. A composite view of the growth rates of the various modes, as a function of a and h, is given in Figure 9. For a range of value of a, the wake modes are more unstable than the boundary layer mode at all wake height. The wake modes become less unstable than the boundary layer mode for cases where wakes with small velocity defect are placed close to the wall, i.e., cases with low values of a and h. For cases with higher values of a, for example, 0.6 and 0.8, the spatial growth rates of the wake modes remain higher than that of the boundary layer mode even at the lowest wake height.

Figures 8 and 9 suggest that for low velocity defect, Mode 1 is more unstable than the antisymmetric Mode 2 for all the wake height. The trend is then reversed when the velocity defect increases. In Figure 10 the effect of the wake velocity defect on the growth rate of Modes 1 and 2 are shown for $h = 20$. The growth rate of Mode 1 is higher than that of Mode 2 for the low values of a and increases nearly linearly with a. The growth rate of Mode 2 is smaller than that of Mode 1 for the lower a, but increases rapidly as the value of a increases. Mode 2 becomes more unstable than Mode 1 for a higher than about 0.5. In other words, there is a switching of the relative level of the spatial growth rate between Mode 1 and Mode 2 based on the present confluent wake/boundary layer model. Calculations using the

measured velocity profile[5] in the very near wake region where the velocity defect is high also show a similar unstable mode switching behavior between the symmetric and the antisymmetric modes. These results seem to indicate that the antisymmetric mode, which generates "puffing" disturbances, is possible to be observed in the near wake immediately downstream of the wake-generating body.

The unstable frequency spectra for Mode 1 and Mode 2 are examined and shown in Figure 11 for $R_e^* = 998$ and for a = 0.4, 0.6, and 0.8. The unstable mode switching appears to have occurred only at low frequency range for a = 0.6 and 0.8. The frequencies for the most unstable waves for both Modes 1 and 2 decrease slightly as a increases. The growth rate for the most unstable Mode 1 is higher than that of Mode 2 for all the a values tested.

Figure 12 shows the real part of the eigenfunctions of Modes 1 and 2 for $R_e^* = 998$, $\omega = 0.1122$, and $a = 0.4$. The eigenfunctions have been normalized by their respective highest amplitudes. It is apparent that the shapes of the eigenfunctions of the wake modes are not strongly dependent upon the wake height.

4. Concluding Remarks

A linear spatial viscous instability analysis for incompressible confluent wake/boundary layer flows has been performed. The global numerical solution tool is validated by comparisons with available data. Two types of discrete unstable modes are identified, which are rooted, respectively, to the boundary layer and the wake parts of the flow model. It is found that the critical Reynolds number associated with the boundary layer mode is reduced by the presence of the wake. The presence of the wake above the boundary layer appears to have an amplifying effect on the growth rate of the boundary layer mode. It is also shown that such an amplifying effect intensifies with an increase of the wake velocity defect. The mode shape of the boundary layer mode also seems to diminish above the wake, indicating that the wake has a confining influence on the disturbances associated with the boundary layer mode. The results suggest that the wake may play an important role in the growth of the linear disturbances and the initiation of transition in the boundary layer. The unstable modes associated with the wake are stabilized by the reduced wake height. An unstable mode switching of the symmetric and the antisymmetric modes is found to occur for low frequency wake modes for cases with high velocity defects, indicating a possible appearance of antisymmetric "puffing" disturbance immediately downstream of the wake-generating body.

Acknowledgement

This work is supported by NASA Langley Research Center under a grant NAG 1-1979. The technical monitor is Dr. C.L. Rumsey.

References

[1]Schlichting, H., *Boundary Layer Theory, McGraw Hill*, 1951.

[2]Tellmien, W., "The Production of Turbulence," NACA TH609, 1931.

[3]Liou, W. W., Fang, Y. C. and Baty, R. S., "Global Numerical Prediction of Bursting Frequency in Turbulent Boundary Layer," Journal of Numerical Methods for Heat and Fluid Flow, Vol. 10, 2000, pp. 862-876.

[4]Sato, H., and Kariki, K., "The Mechanism of Transition in the Wake of a Thin Flat Plate Placed Parallel to a Uniform Flow," Journal of Fluid Mechanics, Vol. 11, 1961, pp. 321-352.

[5]Mattingly, G. E., and Criminale, W. O., "The Stability of an Incompressible Two-Dimensional Wake," Journal of Fluid Mechanics, Vol. 51, 1972, pp. 233-272.

[6]Hultgren, L. S., and Aggarwal, A. K., "Absolute Instability of the Gaussian Wake Profile," Physics of Fluids. Vol. 30, No. 11, 1987, pp. 3383-3387.

[7]Monkewitz, P. A., and Nguyen, L. N., "Absolute Instability in the Near-Wake of Two-Dimensional Bluff Bodies," Journal of Fluids and Structures, Vol. 1, 1987, pp. 165-184.

[8]Bajwa, A. R., "Instabilities Induced by Fixed and Free Particles in a Boundary Layer," Ph. D thesis, Penn State University, December, 1995.

[9]Chin, V., Peters, D., Spaid, F., and McGheo, R., "Flow Field Measurements about a Multi-Element Airfoil at High Reynolds Numbers," AIAA paper 93-3137, 1993.

[10]Bertelrud, A., "Transition on a Three-Element High Lift Configuration at High Reynolds Numbers," AIAA paper 98-0703, 1998.

[11]Roback, V. E., Dam, C. P. van, Los, S. M., Yip, L. P., and Banks, D. W., "Attachment-Line Transition and Boundary Layer Relaminarization on a High Lift Wing in Flight," SAE paper 965564, 1996.

[12]Butter, D. J., "Recent Progress on Development and Understanding of High Lift Systems," AGARD 365, 1984.

[13]Dam, C. P. van, Los, S. M., Miley, S. J., Roback, V. E., Yip, L. P., Bertelrud, A., and Vijgen, P. M. H. W., "In-Flight Boundary Layer State Measurements on a High Lift System: Slat," Journal of Aircraft, Vol. 34, No. 6, 1997, pp. 748-756.

[14]Pobrzynski, W., Nagakura, K., Gohlhar, B., and Buschbaum, A., "Airframe Noise Studied in Wings with Deployed High-Lift Devices," AIAA paper 98-2337, 1998.

[15]Liou, W. W., and Liu, F. J., "Computational Modeling for the Transitional Flow over a Multi-Element Airfoil," AIAA paper 2000-4322, 2000.

[16]Rumsey, C. L. and Gatski, T. B., "Recent Turbulence Model Advances Applied to Multi-Element Airfoil Computations," AIAA paper 2000-4323, 2000.

[17]Bridges, T. J., and Morris, P. J., "Differential Eigenvalue Problems in Which the Parameter Appears

Nonlinearly," Journal of Computational Physics, Vol. 55 , 1984, pp. 437-460.

[18]Joslin, R. D., and Chang, C. L., "Validation of Three-Dimensional Incompressible Spatial Direct Numerical Simulation Code," NASA Technical Paper 3205, 1992.

[19]Liou, W. W., and Morris, P. J., "The Eigenvalue Spectrum of the Reyleigh Equation for a Plane Shear Layer," International Journal of Numerical Methods in Fluids, Vol.15, 1992, pp. 1407-1415.

[20]Morris, P. J., "Stability of a Two-Dimensional Jet," AIAA Journal, Vol. 19, 1981.

[21]Lancaster, P., *Lambda Matrix and Vibrating Systems, Permagon*, Oxford, 1966.

[22]Jordinson, R., "The Flat Plate Boundary Layer, Part 1: Numerical Integration of the Orr-Sommerfeld Equation," Journal of Fluid Mechanics, Vol. 43, 1970, pp. 801-811.

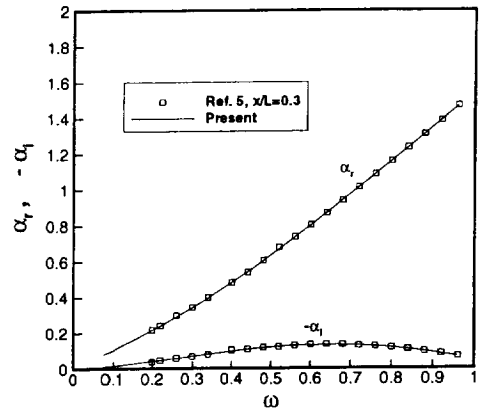

Figure 2(a).

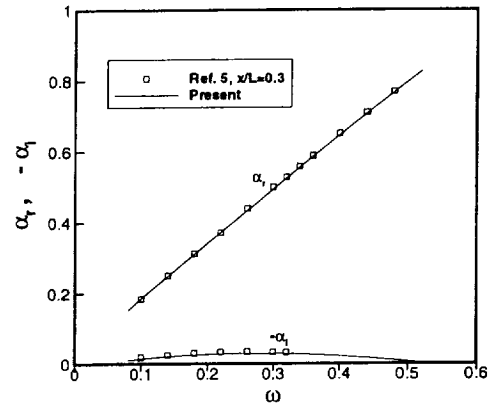

Figure 2(b).

Figure 2. Dispersion relation for wake modes. (a) Symmetric; (b) Antisymmetric.

Table 1. Eigenvalues. $R_e^* = 998$, $\omega = 0.1122$, $\alpha = 0.3086 - i\,0.0057$ (Jordinson[22]).

N	γ	α
36	0.998	0.308444 – i 0.005965
41	0.998	0.308599 – i 0.005662
51	0.998	0.308607 – i 0.005698
61	0.998	0.308597 – i 0.005707
71	0.998	0.308592 – i 0.005707
81	0.997	0.308591 – i 0.005704
91	0.994	0.308590 – i 0.005704
101	0.992	0.308590 – i 0.005704

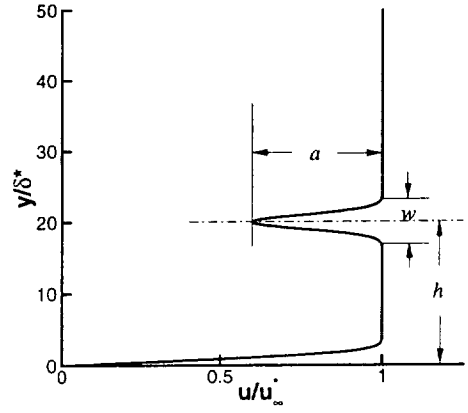

Figure 1. Flow Model.

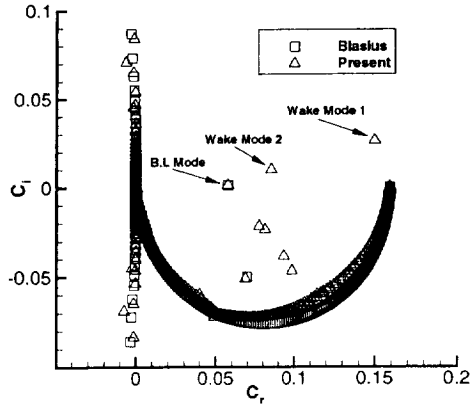

Figure 3. Eigenvalue Spectra. h=20, ω= 0.1122, a=0.6.

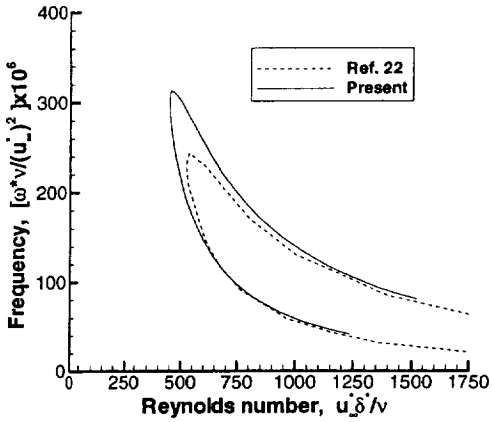

Figure 4. Neutral curves for the boundary layer mode. $a = 0.6$, h=7.14.

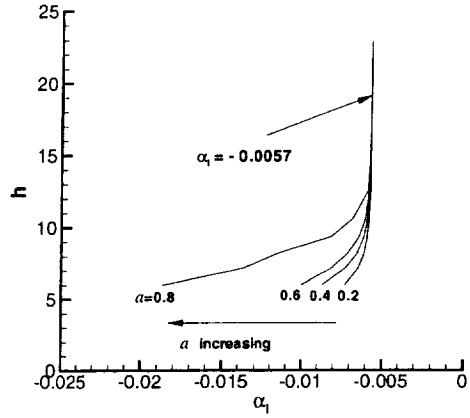

Figure 7. Growth rates for the boundary layer mode. $R_e^* = 998$, $\omega = 0.1122$.

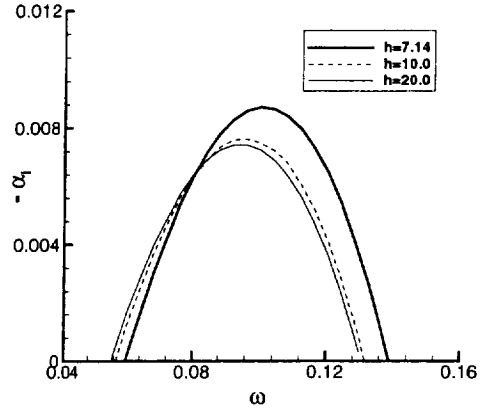

Figure 5. Growth rates for the boundary layer mode. $R_e^* = 998$, $a = 0.6$.

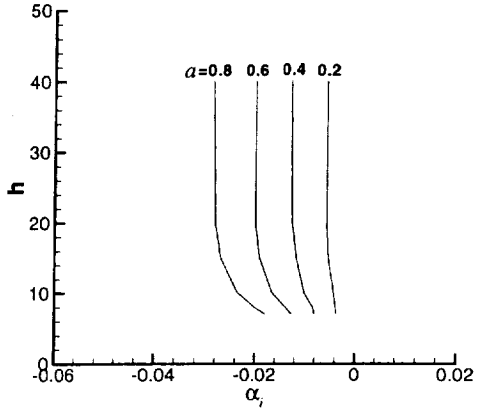

Figure 8(a).

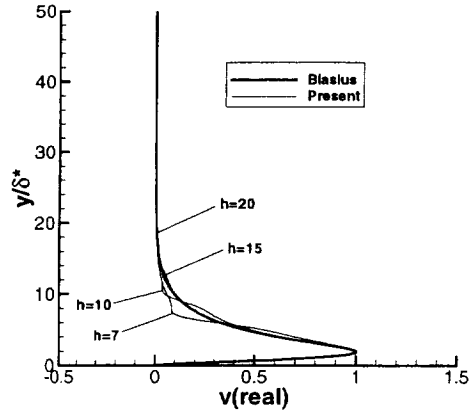

Figure 6. Eigenfunctions for the boundary layer mode. $R_e^* = 998$, $\omega = 0.1122$.

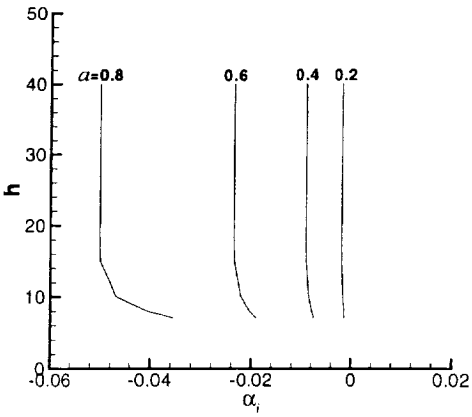

Figure 8(b).

Figure 8. Effect of h and a on the wake modes. $R_e^* = 998$, $\omega = 0.1122$. (a) Mode 1; (b) Mode 2.

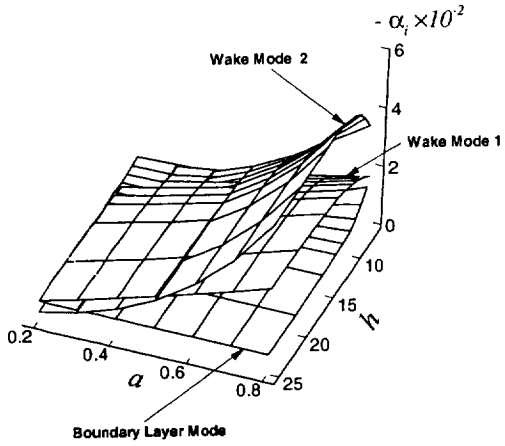

Figure 9. A composite view of the growth rates of the various modes.

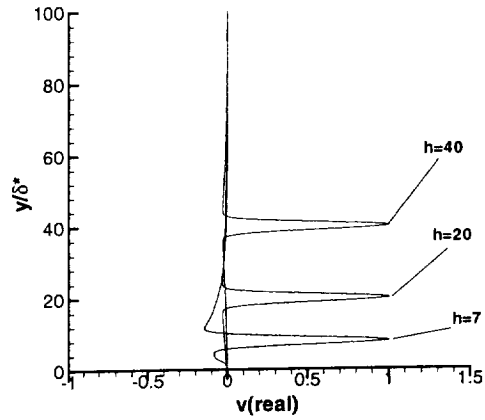

Figure 12(a).

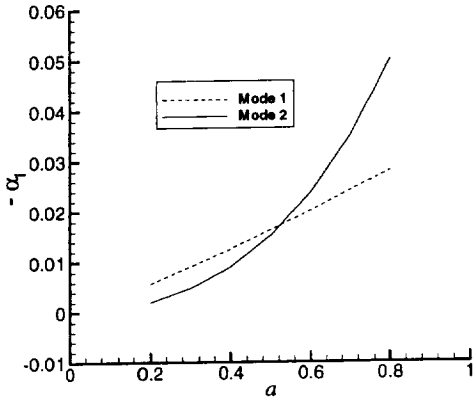

Figure 10. Unstable mode switching.
$R_e^* = 998$, $\omega = 0.1122$.

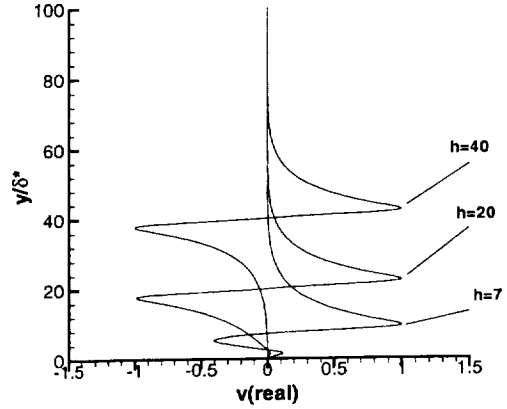

Figure 12(b).

Figure 12. Eigenfuctions for Modes 1 and 2.
$R_e^* = 998$, $\omega = 0.1122$, $a = 0.4$.
(a) Mode 1; (b) Mode 2.

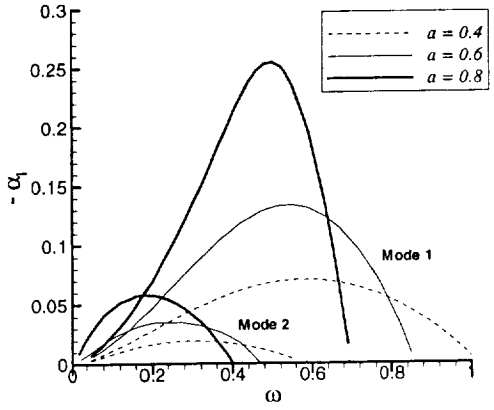

Figure 11. Growth rates of Modes 1 and 2.
$R_e^* = 998$, h=20.